Time-resolved photofragmentation of stored silver clusters Ag_n^+ $(n=8-21)$

U. Hild,[1,*] G. Dietrich,[2,†] S. Krückeberg,[1] M. Lindinger,[1,‡] K. Lützenkirchen,[2] L. Schweikhard,[1] C. Walther,[2] and J. Ziegler[1,§]

[1]*Institut für Physik, Universität Mainz, D-55099 Mainz, Germany*

[2]*Institut für Kernchemie, Universität Mainz, D-55099 Mainz, Germany*

(Received 3 November 1997)

The time-resolved decay of silver clusters Ag_n^+ $(n=8-21)$ has been observed after excitation by photons with energies 1.5–4 eV. Clusters were found to decay by emission of neutral atoms or dimers with lifetimes in the range 100 μs to 15 ms. Separation energies were calculated from the lifetimes assuming a statistical unimolecular decay. As a function of cluster size, the resulting values increase towards the bulk cohesive energy of silver. They show a pronounced odd-even alternation and an indication of a shell closure at $n=9$. The separation energies for $n=8,9$ are in good agreement with configuration-interaction *ab initio* calculations. [S1050-2947(98)05504-8]

PACS number(s): 36.40.Qv, 36.40.Wa

I. INTRODUCTION

The separation (or dissociation) energy of a cluster, required to remove an atom, is one of the basic properties describing its stability [1–14]. It has an influence on the chemistry of clusters, with a low separation energy indicating a facile breaking of bonds and thus a high chemical reactivity [15]. The size dependence of the separation energy is connected to the evolution of atomic to bulk properties. For smaller clusters discontinuities and eletronic shell effects have been observed, for larger ones with some tens of atoms a monotonic increase following a liquid drop behavior [9]. Through a comparison with theoretical calculations of the total binding energy [16], separation energies may serve to gain information on the geometrical structure of a cluster.

One way to measure separation energies is by collision-induced dissociation (CID) where clusters are excited by single or multiple collisions with neutral atoms [2–6]. Depending on the respective collision impact parameters, a broad distribution of excitation energies is populated. Separation energies are inferred from the onset of the fragmentation yield measured as a function of the collision energy.

Another technique is photoabsorption [7–14], which offers the advantage that clusters may be excited by a known amount of energy above the fragmentation threshold. The electronic excitation is converted into a vibrational one and the clusters decay with lifetimes depending on the energy deposited in excess of the separation energy [17,18]. Hence, by measuring lifetimes of excited clusters at a given photon energy, the separation energies may be determined [10–12,14].

Based on these two approaches, separation energies have been determined for a number of alkali [7–9] and transition metals [2–5,10–14]. In the case of the Ib elements copper [11], silver [14], and gold [5,12–14], the electronic structures resemble those of the alkali metals: Each of the ground-state atoms has a closed *d* shell and a single *s* valence electron. Among these silver clusters are of particular practical interest due to their role in photographic processes [19–21]. From a theoretical viewpoint reliable predictions of the electronic and geometric structure of silver clusters may be obtained more easily as compared to copper and gold clusters, which require an explicit treatment of correlation effects for *d* electrons [16].

Various properties of silver clusters have been examined already. From abundance spectra odd-even alternations and shell effects are known [22–24], which were explained in a one-electron shell model as in the case of alkali-metal clusters. Additional electronic properties were studied, such as ionization potentials [25,26], electron affinities [27–29], and the optical response of charged clusters [14,30,31]. In a quadrupole drift tube the decay channels of silver clusters were determined after photoexcitation [32,33]. With Ag_3^- stored in a quadrupole ion trap, the internal motion of Ag_3 could be studied using femtosecond laser spectroscopy and successive ionization to yield Ag_3^+ [34]. Recently, the decay paths of Ag_n^+ [35] and Ag_n^{2+} clusters [36–38] were determined by CID in a Penning trap. With a configuration-interaction (CI) *ab initio* method the structures, the total binding energies, and the ionization potentials were calculated for small neutral and charged silver clusters [16,39].

In this article we report on the photofragmentation of Ag_n^+ clusters $(n=8-21)$ stored in a Penning trap. With the storage technique the decay of excited clusters can be followed over a broad time scale $10^{-5}-10^{-1}$ s. This allows us to determine cluster separation energies with high accuracy. Sections II and III give an overview of the experimental approach and the measurements. Section IV covers the determination of separation energies from the decay of the parent clusters, the sequential decay of excited fragments, and a discussion of decay channels of Ag_{13}^+. Conclusions are given in Sec. V.

*Present address: IBM Deutschland Entwicklung GmbH, D-71032 Böblingen, Germany.

†Present address: SerCon GmbH, D-55130 Mainz, Germany.

‡Present address: Frankfurter Allgemeine Zeitung, D-60267 Frankfurt, Germany.

§Present address: Deutsche Bank AG, D-60325 Frankfurt, Germany.

 © 1998 The American Physical Society

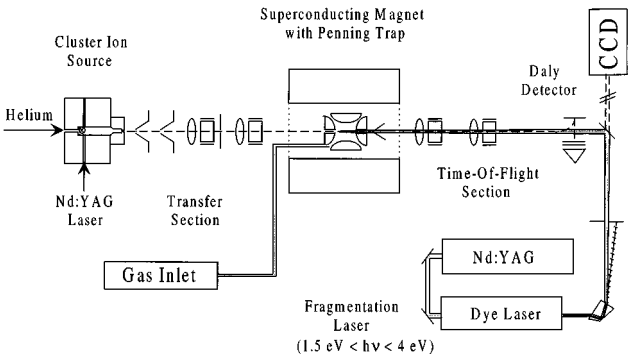

FIG. 1. Schematic overview of the experimental setup: Metal clusters are produced in an external ion source and guided by ion-optical elements to a Penning trap, located in the bore of a 5-T magnet. Fragmentation of clusters is induced by absorption of photons from a Nd:YAG dye laser system. The position of the laser beam relative to the cluster ion cloud is monitored by a CCD camera. To measure lifetimes of clusters as a function of internal energies, all ions are ejected out of the trap at variable times after laser irradiation and are detected by time-of-flight mass spectrometry.

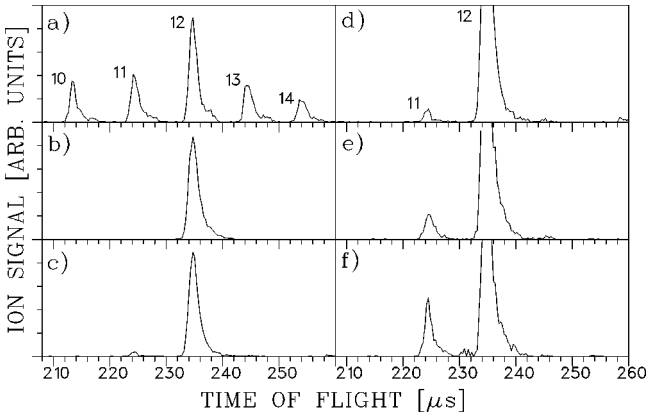

FIG. 2. For the photofragmentation of Ag_{12}^{+} time-of-flight spectra are shown that illustrate the experimental sequence: (a) capture of a distribution of Ag_n^{+} clusters around Ag_{12}^{+} and centering of Ag_{12}^{+} by collisional cooling; (b) mass separation of Ag_{12}^{+} by radial ejection of all other clusters; (c) fragmentation of Ag_{12}^{+} into Ag_{11}^{+} induced by 2.30-eV photons at $\Delta t = 1$ μs between the laser pulse and TOF analysis; (d) same as (c) with the y axis stretched by a factor of 3; (e) $\Delta t = 3$ ms; (f) $\Delta t = 40$ ms.

II. EXPERIMENT

The Penning trap mass spectrometer constructed for experiments with stored cluster ions has been described in detail in Ref. [40]. Its main features are reviewed briefly (Fig. 1), while characteristics of the present measurements are presented in more detail.

Positively charged silver clusters are produced by laser vaporization of a silver wire and condensation in a helium gas pulse. They are guided towards a Penning trap whose electrode configuration consists of a segmented ring and two end caps. Each end cap has a hole in the center in order to inject (eject) the clusters into (out of) the trap. The capture of clusters is performed by lowering the potential of the entrance end cap down to the value of the ring electrode when the ions are arriving and increasing it back to the trapping value when they are inside the trap. The size distribution of the captured clusters [Fig. 2(a)] is adjusted by suitable potential differences between the cluster source and Penning trap. Ions are stored by superposition of a homogeneous magnetic field ($B = 5$ T) for radial and an electric-quadrupole field for axial confinement. The depth of the electrostatic potential well in the axial direction is 1.5 V. In the following, one experimental cycle for measuring the photofragmentation of Ag_n^{+} clusters is described. The time duration of one cycle is 780 ms. Typically, the data of 200 cycles with 20–50 cluster ions each are added to obtain statistically significant signal intensities.

In order to optimize the fragmentation yield and the overlap with the laser beam (see below) clusters of the size to be studied are centered in the middle of the trap. This is achieved by a combination of collisional energy loss and rf excitation at their cyclotron frequency $\omega_c = qB/M$ (q is the ion charge and M is the ion mass) [41]: To induce collisions, four pulses of argon are injected through a piezoelectric

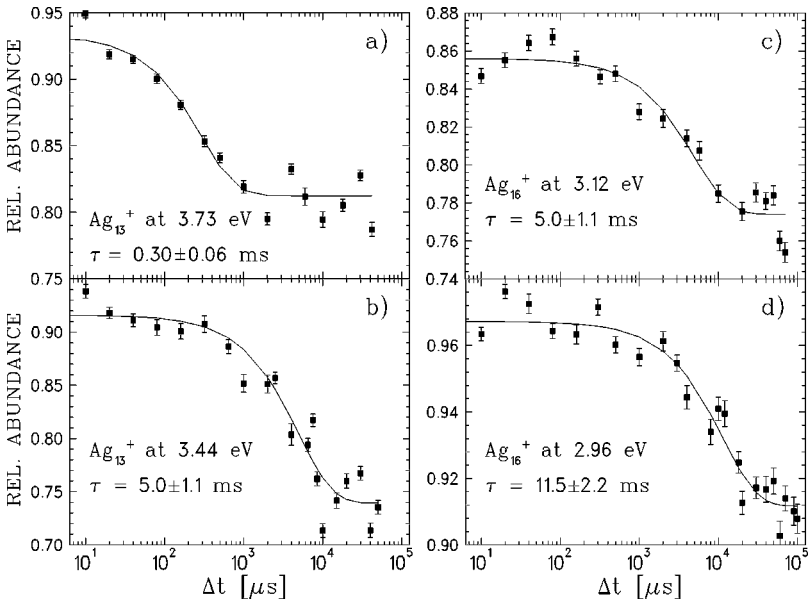

FIG. 3. Relative cluster abundances as a function of time Δt between the laser pulse and the time-of-flight measurement: Ag_{13}^{+} at photon energies of (a) 3.73 eV and (b) 3.44 eV and Ag_{16}^{+} at photon energies of (c) 3.12 eV and (d) 2.96 eV. The solid lines are exponential functions fitted to the data.

TABLE I. Measured time constants τ_n for fragmentation of Ag_n^+ at different laser wavelengths λ and photon energies $h\nu$. τ_{n-1} and τ_{n-2} represent the time constants for formation of the fragments Ag_{n-1}^+ and Ag_{n-2}^+. An empty entry indicates that no time dependence was observed.

n	λ (nm)	$h\nu$ (eV)	τ_n (ms)	τ_{n-1} (ms)	τ_{n-2} (ms)
8	603	2.06	0.21 ± 0.03	0.21 ± 0.03	
9	408	3.04	0.53 ± 0.12	0.57 ± 0.11	
	419	2.96	0.52 ± 0.13	0.55 ± 0.11	
10	710	1.75	0.33 ± 0.07	0.31 ± 0.07	
	780	1.59	11.1 ± 2.9	11.1 ± 2.9	
11	430	2.88	0.11 ± 0.04		0.12 ± 0.04
	440	2.82	0.13 ± 0.05		0.12 ± 0.05
	450	2.78	1.5 ± 0.6		1.3 ± 0.5
12	530	2.34	1.9 ± 0.6	1.9 ± 0.6	
	540	2.30	3.2 ± 0.8	4.9 ± 0.9	
13	332	3.73	0.30 ± 0.06	0.26 ± 0.05	0.35 ± 0.12
	360	3.44	5.0 ± 1.1	3.6 ± 0.6	10.0 ± 5.9
14	430	2.88	1.4 ± 0.2	2.5 ± 0.3	0.23 ± 0.08
	450	2.76	2.8 ± 1.0	6.0 ± 1.3	1.2 ± 0.3
15	310	4.00	13.5 ± 6.2	3.4 ± 0.7	2.8 ± 0.8 [a]
	333	3.72	5.8 ± 2.9	10.7 ± 1.5	
16	398	3.12	5.0 ± 1.1	11.9 ± 1.4	2.0 ± 0.4
	419	2.96	11.5 ± 2.2	14.1 ± 2.9	6.2 ± 1.5
17	545	2.28	2.5 ± 0.9	1.2 ± 0.3	
18	545	2.28	0.12 ± 0.04	0.09 ± 0.03	1.9 ± 0.5
19	485	2.56	7.3 ± 2.3	10.5 ± 2.4	
20	530	2.34	1.7 ± 0.6	0.64 ± 0.15	[b]
	540	2.30	1.1 ± 0.3	0.81 ± 0.16	[b]
21	408	3.04	0.14 ± 0.03	0.11 ± 0.02	
	428	2.90	0.29 ± 0.12	0.35 ± 0.05	

[a]Time constant for the *decay* of the Ag_{13}^+ fragment cluster.

[b]A time dependence for the Ag_{18}^+ fragments was observed, but the uncertainties of the data are too large to determine a time constant.

valve installed near the trap. The rf excitation is applied for 650 ms and covers the range of cyclotron frequencies that correspond to the isotopic mass distribution of the given cluster size. The spatial cluster distribution after centering was determined from the fragmentation yield measured with a narrowly focused laser beam of 0.3 mm diameter. The distribution along the horizontal and vertical axes through the center of the trap was found to follow a Gaussian with a diameter [full width at half maximum (FWHM)] of 1.8 mm. Due to the buffer gas collisions the clusters may well be expected to be in thermal equilibrium with the gas molecules at 300 K.

The cluster size in question is mass selected by radial ejection of all other ions [Fig. 2(b)]. To induce fragmentation of clusters, the light of a pulsed dye laser (Lambda Physik, FL 2001, pulse length 10 ns), which is pumped by the second or third harmonic of a Nd:YAG laser (where YAG denotes yttrium aluminum garnet) (Lumonics, HY 400), is focused axially into the Penning trap. By frequency doubling with a β-barium-borate crystal photons in the energy range 1.5–4 eV are produced. The laser wavelengths are adjusted with an accuracy of 0.01 nm using a pulsed wavemeter (Burleigh Instruments WA-4500). The charged fragmentation products [Fig. 2(c)] are axially ejected and identified by time-of-flight (TOF) mass spectrometry. Single-ion detection is performed by use of a conversion dynode detector. Its aluminum electrode and microchannel plate detector are mounted off the cluster beam axis in order to axially focus the fragmentation laser beam into the trap (Fig. 1). The number of cluster ions was chosen low enough to avoid saturation effects of the detection system. The time evolution of the fragmentation processes is studied by variation of the storage time Δt (typically 20 μs to 100 ms) between laser excitation and ejection of the product ions out of the trap.

In order to control the position of the laser beam relative

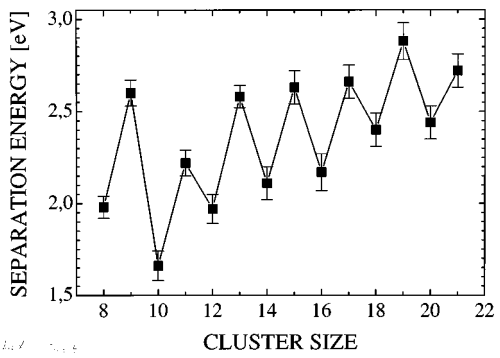

FIG. 4. Separation energies of Ag_n^+, $n=8-21$, calculated with Eq. (2) from the lifetimes τ_n of the parent clusters (Table I).

TABLE II. Separation energies D_n^+ of Ag_n^+ clusters at different photon energies $h\nu$. The last column gives the average values $\overline{D_n^+}$. The D_n^+ values are calculated with Eq. (2) assuming a one-photon absorption for the cluster sizes $n=8-16$ and a two-photon absorption for the sizes $n=17-21$. Clusters that evaporated a dimer are marked with (D). For all other cluster sizes evaporation of monomers was observed.

n	$h\nu$ (eV)	D_n^+ (eV)	$\overline{D_n^+}$ (eV)
8	2.06	1.98 ± 0.06	1.98 ± 0.06
9	3.04	2.62 ± 0.07	2.60 ± 0.07
	2.96	2.57 ± 0.07	
10	1.75	1.64 ± 0.07	1.66 ± 0.08
	1.59	1.67 ± 0.08	
$11^{(D)}$	2.88	2.21 ± 0.07	2.22 ± 0.07
	2.82	2.18 ± 0.07	
	2.76	2.28 ± 0.08	
12	2.34	1.97 ± 0.08	1.97 ± 0.08
	2.30	1.97 ± 0.08	
13 [a]	3.73	2.57 ± 0.06	2.58 ± 0.06
	3.44	2.59 ± 0.06	
$13^{(D)}$, [a]	3.73	2.62 ± 0.10	2.64 ± 0.10
	3.44	2.66 ± 0.10	
14	2.88	2.12 ± 0.09	2.11 ± 0.09
	2.76	2.09 ± 0.09	
15	4.00	2.66 ± 0.09	2.63 ± 0.09
	3.72	2.60 ± 0.09	
16	3.12	2.18 ± 0.09	2.17 ± 0.10
	2.96	2.15 ± 0.10	
17	2.28	2.66 ± 0.09	2.66 ± 0.09
18	2.28	2.40 ± 0.09	2.40 ± 0.09
19	2.56	2.88 ± 0.10	2.88 ± 0.10
20	2.34	2.44 ± 0.09	2.44 ± 0.09
	2.30	2.43 ± 0.09	
21	3.04	2.71 ± 0.09	2.72 ± 0.09
	2.90	2.72 ± 0.09	

[a]For the calculation of $D_{13,1}^+$ and $D_{13,2}^+$ see Sec. IV C.

to the cluster ion cloud as well as the laser-beam shape, 5% of the light is reflected to a charge coupled device (CCD) camera and monitored on line by a beam profile analyzing system (Laser 2000, BIG SKY). Typical values are a profile of 95% Gaussian shape with 1.5–2.5 mm diameter (FWHM) and pulse energies covering a range from about 100 μJ to 2 mJ.

III. MEASUREMENTS AND RESULTS

The aim of the present experiment is to measure the fragmentation time dependence for a size-selected ensemble of photoexcited Ag_n^+ clusters. A Penning trap is well suited for such a measurement since all charged products remain stored until they are ejected for the purpose of a TOF analysis. By variation of the storage duration Δt between laser excitation and ion ejection the fragmentation time dependence is determined from the respective numbers of Ag_n^+ clusters and fragmentation products, $Ag_{m<n}^+$. As an example, Figs. 2(d)–2(f) show TOF spectra of the photofragmentation of Ag_{12}^+ for different storage times Δt. The relative abundance of the Ag_{11}^+ fragment increases for larger values of Δt.

For Ag_{13}^+ and Ag_{16}^+ as examples, Figs. 3(a)–3(d) depict the decrease of the relative parent cluster abundances as a function of Δt for fragmentation with two different photon energies. (The corresponding increase of the fragment ions is discussed in Sec. IV B; see Figs. 5 and 6.) The error bars correspond to the 1σ statistical uncertainties. The solid lines are exponential functions fitted to the data by χ^2 minimization. The fitting function has the form

$$y(\Delta t)=ae^{-\Delta t/\tau}+b, \tag{1}$$

where τ is the lifetime of parent clusters, $a+b$ is their relative abundance for $\Delta t<10^{-5}$ s, and b is their relative abundance for large Δt, i.e., the fraction of clusters that did not absorb a photon. Typically, the relative magnitude of the delayed fragmentation, viz. a, is 5–10 %. It was kept this low on purpose in order to minimize the probability for multiple photon absorption.

With increasing photon energy the lifetimes decrease considerably. The photon energies were chosen such that fragmentation occurred within the experimentally accessible time range $\Delta t\simeq 10^{-5}-10^{-1}$ s. The lower limit is determined by the extraction time of the clusters from the trap for TOF analysis; all clusters that decay within 10^{-5} s after the laser pulse are detected as fragments. The upper limit is set by the pressure in the Penning trap ($\simeq 10^{-7}$ mbar) since the photoexcited clusters may lose internal energy upon collisions

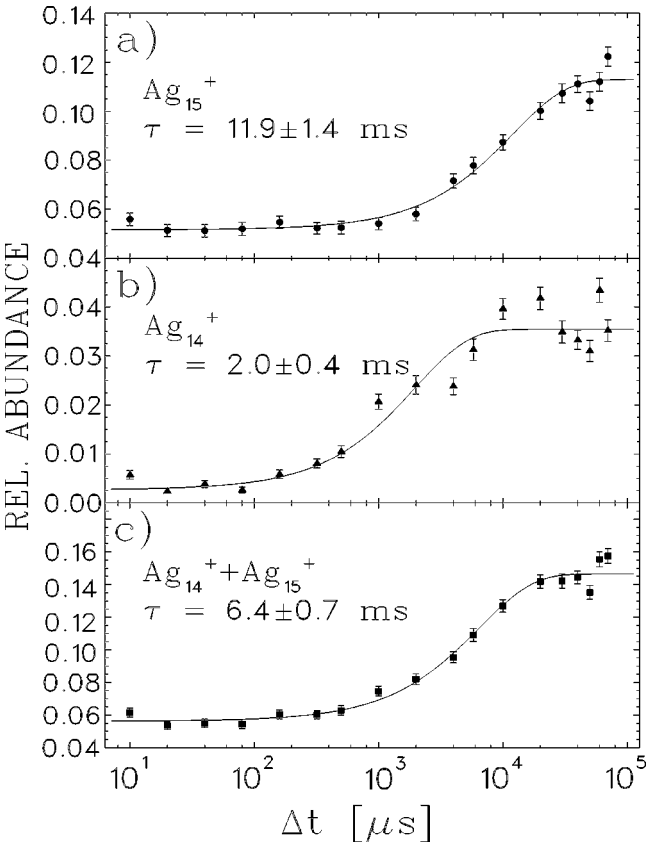

FIG. 5. Relative abundances of (a) Ag_{15}^+ and (b) Ag_{14}^+ fragments resulting from the decay of Ag_{16}^+ at 3.12-eV photon energy as a function of time Δt. (c) is the sum of (a) and (b).

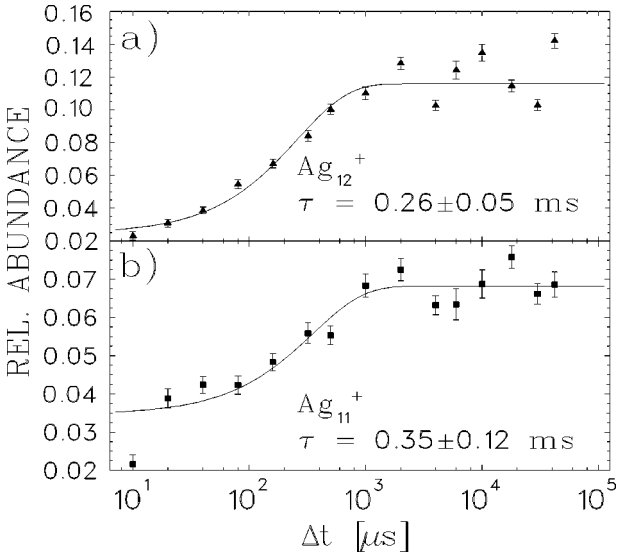

FIG. 6. Relative abundances of (a) Ag_{12}^+ and (b) Ag_{11}^+ fragments resulting from the decay of Ag_{13}^+ at 3.73-eV photon energy as a function of time Δt.

with gas atoms. In addition, energy loss by emission of infrared radiation is likely to gain importance on the time scale of several tens of milliseconds [42,43].

Note that the relative abundances of Ag_{13}^+ and Ag_{16}^+ are less than 100% at small Δt. This is due to the absorption of two or more photons by a single cluster and its subsequent fragmentation within a time shorter than 10 μs.

Lifetimes of photoexcited clusters were measured for Ag_n^+, $n=8-21$. For smaller clusters photofragmentation occurred, but no time dependence was observed in the range of photon energies studied here. Possibly, photodissociation might proceed directly via a repulsive potential for these smaller clusters [11].

The fragmentation time constants for the photon energies and cluster sizes studied are summarized in Table I. For most cluster sizes measurements have been performed with at least two different photon energies. The measured time constants cover the range from about 10^{-4} s to 10^{-2} s. The τ_n values are time constants for fragmentation of the parent clusters. The values of τ_{n-1} for clusters with $n=8$–10,12 represent the formation of fragment clusters due to monomer evaporation; for $n=11$ only fragments due to dimer evaporation with time constant τ_{n-2} were observed. Note that in these cases $\tau_n \simeq \tau_{n-1}$ and $\tau_n \simeq \tau_{n-2}$, respectively, within experimental errors. The data for $n=13$ are consistent with a competition between monomer (τ_{n-1}) and dimer (τ_{n-2}) evaporation; see Sec. IV C. Clusters with $n \geq 14$ generally decay by emission of monomers with the decay described by the τ_n values only. The fragments formed by the loss of two atoms are due to a sequential decay. Hence the data for the first fragment are a convolution of formation and decay; the corresponding τ_{n-1} values have no direct physical meaning and are only given in the sense of a fit parameter; see Sec. IV B.

The fragmentation channels observed are in line with earlier results for the collision-induced fragmentation of Ag_n^+, $n=3$–20 [35]: For $n=3,5,7,11$ dimer emission was found, the data for $n=13$ indicate a coexistence of monomer and dimer emission, and all other clusters preferentially decay by emission of monomers.

IV. DISCUSSION

A. Separation energies

The measured lifetimes of the fragmentation processes yield information on the separation energies of the clusters. While the laser pulse has a length of about 10 ns, the observed decays occur on time scales that are four to six orders of magnitude larger. One may safely assume that the initial electronic excitation has been converted to vibrational excitation during this period. The decay process may thus be described by a statistical unimolecular dissociation. An appropriate approach for the present problem is the quantum version of Kassel's theory [17,18]. The more sophisticated theory of Rice, Ramsperger, Kassel, and Marcus [44] requires knowledge of the vibrational density of states, little of which is known for the clusters in question. Within Kassel's approach, s oscillators of frequency ν share a number of $p=E_n^*/h\nu$ quanta; E_n^* represents the vibrational excitation energy for an n-atom cluster. Dissociation occurs if one oscillator contains at least $q=D_{n,m}^+/h\nu$ quanta; $D_{n,m}^+$ represents the separation energy of Ag_n^+ for the decay $Ag_n^+ \rightarrow Ag_{n-m}^+ + Ag_m$. The decay rate, which is the inverse of the measured lifetime, follows as

$$k_n(ph\nu)=\tau_n^{-1}=g\nu\frac{p!(p-q+s-1)!}{(p-q)!(p+s-1)!}, \tag{2}$$

with a degeneracy factor g. For g, values of n (for $n=8$–12), $n-1$ (for $n=13$), and $n-2$ (for $n=14$–21) are chosen. This choice, however, is not crucial. As an example, a variation of $\Delta g = 2$ results in an uncertainty of less than 0.02 eV for the separation energy of Ag_{14}^+. The oscillator frequency ν is approximated by the Debye frequency of silver, 4.70×10^{12} Hz [45]. The excitation energy E_n^* is given by the sum of the thermal energy of the cluster before the laser irradiation sk_BT ($s=3n-6$ and $T=300$ K; cf. Sec. II) and the energy gained by photoabsorption

$$E_n^*=\ell h\nu+sk_BT. \tag{3}$$

The number of absorbed photons ℓ was established by requiring consistency of the separation energies from Eq. (2) with theoretical values for $n=8,9$ [16] and relative experimental values for $n=8-21$ determined by CID [46]. Hence $\ell=1$ was used for $n=8-16$ and $\ell=2$ for the larger clusters. This increase of ℓ is due to the increasing number of degrees of freedom: In order to fragment within the experimental time window, more excitation energy is needed for the larger clusters as compared to the smaller ones.

In Table II the separation energies calculated from the observed lifetimes of the parent clusters are given. The errors include an estimated uncertainty of 50 K for the cluster temperature prior to laser irradiation and the uncertainties of the measured lifetimes. Note that in all cases where several wavelengths were used the separation energies agree to within 4%. In Fig. 4 the average separation energies are shown as a function of cluster size.

The D_n^+ values are equivalent to monomer separation energies except in the cases of Ag_{11}^+ and Ag_{13}^+. For the

decay of Ag_{11}^+ the only fragment observed is Ag_9^+, which indicates the emission of a Ag_2 dimer. This finding is consistent with the energy balance for monomer and dimer decay of Ag_n^+. The values of $D_{n,1}^+$ and $D_{n,2}^+$ are given by

$$D_{n,1}^+ = E_{n-1}^+ + E_1 - E_n^+ , \tag{4}$$

$$D_{n,2}^+ = E_{n-2}^+ + E_2 - E_n^+ . \tag{5}$$

E_n^+ and E_n denote the total binding energy of positively charged and neutral n-atom clusters, respectively. With $E_1 = 0$ and $E_2 = -D_2$ one obtains

$$D_{n,2}^+ - D_{n,1}^+ = D_{n-1,1}^+ - D_2 . \tag{6}$$

Since dimer emission predominates for Ag_{11}^+, one has $D_{11,2}^+ < D_{11,1}^+$, which is equivalent to $D_2 > D_{10,1}^+$. Since $D_2 = 1.69 \pm 0.08$ eV [47] and $D_{10,1}^+ = 1.66 \pm 0.08$ eV (Table II) it is apparent that dimer emission is energetically feasible. The case of Ag_{13}^+ is more complicated and will be discussed separately in Sec. IV C.

The separation energies converge towards the bulk cohesive energy of silver (2.95 eV [47]). They show a pronounced odd-even alternation with a higher stability of the even-electron clusters as compared to the odd-electron ones. The same alternation was observed in abundance spectra of Ag_n^+ [22–24]. As argued in Ref. [48] the odd-even staggering is the result of a ground-state deformation of the clusters, which tends to remove all degeneracies except the double spin degeneracy of each level. An odd electron has to enter a higher single-particle level than the previous even electron that filled the doubly degenerate state. An eight-electron shell closure is apparent from the high separation energy for Ag_9^+ and the correspondingly low value for Ag_{10}^+.

The binding energies of Ag_n^+ clusters ($n = 2$–9) were calculated [16] performing CI *ab initio* calculations for several ionic structures. For the most stable structures an odd-even alternation is noticeable with a higher binding energy of the even-electron clusters. For a quantitative comparison with the present experimental data, the calculated binding energies of the most stable Ag_8^+ and Ag_9^+ structures were converted into separation energies. One obtains values of $D_{8,1}^+ = 1.96$ eV and $D_{9,1}^+ = 2.77$ eV, which are in good agreement with the data in Table II. This indicates that for the two clusters in question the calculated most stable structures are indeed the energetically favorable ones.

B. Sequential decays

If a cluster absorbs more than one photon its internal energy may be sufficiently high for evaporation of several atoms. Figures 3(c), 5(a), and 5(b) show an example of such a sequential decay in the case of Ag_{16}^+, i.e.,

$$Ag_{16}^+ \rightarrow Ag_{15}^+ + Ag \rightarrow Ag_{14}^+ + 2Ag.$$

After laser irradiation with 3.12-eV photons the time-resolved decay of Ag_{16}^+ and the formation of Ag_{15}^+ and Ag_{14}^+ are observed. The fitting function used to describe the fragment formation is

$$y(\Delta t) = c(1 - e^{-\Delta t/\tau}) + d, \tag{7}$$

where d is the relative abundance for $\Delta t < 10^{-5}$ s and $c + d$ the relative abundance for large Δt.

TABLE III. Separation energies $D_{n-1,1}^+$ of Ag_{n-1}^+ clusters calculated from sequential decay data. n gives the number of atoms of the parent cluster, ℓ the number of absorbed photons of energy $h\nu$.

$n-1$	n	ℓ	$h\nu$ (eV)	$D_{n-1,1}^+$ (eV)
15	16	2	3.12	2.57 ± 0.13
15	16	2	2.96	2.49 ± 0.13
17	18	3	2.28	2.47 ± 0.13

The various decay times and cluster abundances can be understood in terms of the number of absorbed photons: The decay of Ag_{16}^+ with $\tau = 5.0 \pm 1.1$ ms is attributed to a decay after one-photon absorption. At small values of $\Delta t < 10$ μs the Ag_{16}^+ abundance has already decreased to about 85%. This decrease is due to absorption of two or more photons and a correspondingly rapid decay. In the case of Ag_{15}^+ the increase of the cluster abundance for $\Delta t > 1$ ms is due to the one-photon induced decay of Ag_{16}^+. The fragment abundance of about 5% at $\Delta t < 1$ ms is due to Ag_{16}^+ decay after absorption of two photons. The internal energy of these Ag_{15}^+ fragments is sufficiently high for evaporation of another atom to yield Ag_{14}^+. The increase of the Ag_{14}^+ abundance to a value close to 5% is fully consistent with this picture.

The time constant for the formation of Ag_{15}^+, which is derived from Fig. 5(a), is of course affected by the sequential decay into Ag_{14}^+. The correct time constant is obtained by summation of the data for Ag_{15}^+ and Ag_{14}^+ [Fig. 5(c)], viz. $\tau = 6.4 \pm 0.7$ ms. Within the uncertainties, this value agrees well with the decay time of Ag_{16}^+.

The above reasoning is further substantiated by a calculation of $D_{n-1,1}^+$ from the data of the sequential Ag_n^+ decay. As will be shown, the resulting value is in complete agreement with the one obtained by direct observation of the Ag_{n-1}^+ decay. The excitation energy of a Ag_n^+ cluster after absorption of ℓ photons is given by Eq. (3). The internal energy of the fragment cluster after emission of an atom is

$$E_{n-1}^* = E_n^* - D_{n,1}^+ - 2k_B T_{fr} , \tag{8}$$

where the average kinetic energy of the emitted atom is $2k_B T_{fr}$ and T_{fr} is the temperature of the fragment cluster [1]. With E_{n-1}^* and the time constant τ_{n-2} for the formation of the second fragment, Eq. (2) yields a value for $D_{n-1,1}^+$. The calculation is performed with several ℓ values to obtain agreement with the data from the direct decay. For example, from the sequential Ag_{16}^+ decay the Ag_{15}^+ separation energy is deduced, $D_{15,1}^+ = 2.7 \pm 0.13$ eV, using $\ell = 2$ and $D_{16,1}^+$ from Table II. (With $\ell = 1$ and 3, on the other hand, one obtains values of 1.1 eV and 4.0 eV.) This value is in good agreement with the result from the direct one-photon-induced Ag_{15}^+ decay of 2.63 ± 0.09 eV.

Several examples of separation energies $D_{n-1,1}^+$ obtained from the sequential decay of Ag_n^+ clusters are listed in Table III. They generally agree well with the results obtained from the direct decay (Table II). This strongly indicates that

the procedure used to derive separation energies from measured time constants is internally consistent.

C. Decay of Ag_{13}^+

For the clusters up to size $n=12$ only one of the fragments, the one with either $n-1$ or $n-2$ atoms, showed a time-dependent formation in the experimentally accessible time range. In these cases, the respective time constants are equal to the decay times of the parent clusters (within experimental uncertainties). For some of the clusters with $n \geqslant 14$ both the $n-1$ and $n-2$ fragments show a time-dependent decay. The time constants are explained in terms of a sequential decay, i.e., the absorption of several photons by the parent cluster and the successive evaporation of two atoms.

In the case of Ag_{13}^+, however, this interpretation does not hold: Figs. 3(a), 6(a), and 6(b) show the decrease of the Ag_{13}^+ signal and the corresponding increase of both the Ag_{12}^+ and Ag_{11}^+ signals as a function of Δt at a photon energy of 3.73 eV. At short Δt (<10 μs) the relative abundance of Ag_{12}^+ is 0.02. These Ag_{12}^+ clusters result from the decay of Ag_{13}^+ after absorption of two or more photons and still carry enough excitation energy to decay into Ag_{11}^+ (cf. Sec. IV B). If all Ag_{11}^+ clusters were due to this kind of sequential decay, their abundance at long Δt should have increased by 0.02 as compared to short Δt. However, the difference in abundances is 0.03–0.05, which shows that Ag_{11}^+ is not (completely) formed by the decay of Ag_{12}^+.

If a sequential decay is still assumed, the separation energy of Ag_{12}^+ may be calculated as described in Sec. IV B. The result is in disagreement with the assumption: The calculated value of $D_{12,1}^+$ is 1.2 eV higher than the one in Table II from the direct one-photon-induced decay of Ag_{12}^+.

Alternatively, the data might be explained by the presence of two Ag_{13}^+ isomers that decay via monomer and dimer evaporation, respectively. The result of almost equal formation times of Ag_{11}^+ and Ag_{12}^+ would in this case be coincidental. In addition, the cluster temperature after absorption of one 3.73-eV photon is on the order of 1500 K. This is higher than the melting temperature of bulk silver, which renders the existence of two isomers highly unlikely. The most plausible explanation of the data is the presence of two coexisting decay channels for Ag_{13}^+, one with monomer the other with dimer evaporation. In this case, the time constants for decay of Ag_{13}^+ and for formation of Ag_{12}^+ and Ag_{11}^+ must be equal. Within uncertainties, this in fact is the case for both photon energies studied (Table I).

The separation energies $D_{13,1}^+$ and $D_{13,2}^+$ are calculated in the following way [49]: The decay rate k_{13} of Ag_{13}^+ is given by the sum of the rates for the monomer and dimer channels

$$k_{13}=k_{13,1}+k_{13,2}. \tag{9}$$

The ratio of $k_{13,1}$ and $k_{13,2}$, on the other hand, is determined by the ratio of the respective channel abundances

$$\frac{k_{13,1}}{k_{13,2}}=\frac{N_{Ag_{12}^+}}{N_{Ag_{11}^+}}. \tag{10}$$

$N_{Ag_{12}^+}$ and $N_{Ag_{11}^+}$ are given by the difference of the abundances at long and short Δt. From Figs. 6(a) and 6(b) one obtains $k_{13,1}/k_{13,2}=2.7\pm0.9$ (at 3.73-eV photon energy). k_{13} is taken as the inverse of the average of the three time constants for the decay of Ag_{13}^+ and the formation of $Ag_{11,12}^+$, $k_{13}=3520\pm450$ s^{-1}. The resulting partial decay rates are $k_{13,1}=2570\pm440$ s^{-1} and $k_{13,2}=950\pm270$ s^{-1}. Assuming decay after one-photon absorption, separation energies are calculated with Eq. (2). One obtains $D_{13,1}^+=2.57\pm0.06$ eV and $D_{13,2}^+=2.62\pm0.10$ eV. The results for a 3.44-eV photon energy are given in Table II. Note that the errors of $D_{13,1}^+$ and $D_{13,2}^+$ are correlated and largely due to the estimated uncertainty of the cluster temperature of 300 ± 50 K. The uncertainty of the difference of the two separation energies is much smaller ($\simeq0.02$ eV).

V. CONCLUSIONS

The time-resolved photofragmentation of Ag_n^+ clusters ($n=8-21$) has been studied on a time scale $10^{-5}-10^{-1}$ s. Clusters were stored in a Penning trap and excited by photons with energies 1.5–4 eV. Parent and fragment clusters were detected by ejection from the trap and time-of-flight mass spectrometry. The decay channels observed are the emission of neutral atoms and dimers with exponential time constants 100 μs to 15 ms.

Separation energies were determined from the measured lifetimes based on the quantum version of Kassel's theory [17,18]. The separation energies converge towards the bulk cohesive energy of silver. They show a pronounced odd-even alternation, which is interpreted in terms of Jahn-Teller deformations [48]. For $n=8,9$ separation energies were calculated with a CI *ab initio* method [16,39]. Good agreement is found between the experimental and theoretical data.

For some of the clusters with $n \geqslant 14$ the sequential evaporation of several atoms was observed (cf. Table I) due to absorption of two or more photons. The calculated separation energies of the first fragments with $n-1$ atoms agree well with values determined from the direct decay of the respective clusters (cf. Tables II and III). Hence the procedure to infer separation energies from measured time constants is internally consistent. In the case of Ag_{13}^+ two competing decay channels were observed, viz., the emission of a neutral atom or a dimer. The respective separation energies were determined from the branching ratio and the time constants.

ACKNOWLEDGMENTS

We thank the Deutsche Forschungsgemeinschaft, the Materialwissenschaftliches Forschungszentrum, Mainz, and the Fonds der Chemischen Industrie for financial support. S.K. and C.W. acknowledge support from the Studienstiftung des Deutschen Volkes and the Graduiertenkolleg ''Physik und Chemie supramolekularer Systeme,'' respectively.

[1] P. C. Engelking, J. Chem. Phys. **87**, 936 (1987).
[2] M. F. Jarrold, J. E. Bower, and J. S. Kraus, J. Chem. Phys. **86**, 3876 (1987).
[3] C.-X. Su and P. B. Armentrout, J. Chem. Phys. **99**, 6506 (1993).
[4] C.-X. Su, D. A. Hales, and P. B. Armentrout, J. Chem. Phys. **99**, 6613 (1993).
[5] St. Becker, G. Dietrich, H.-U. Hasse, N. Klisch, H.-J. Kluge, D. Kreisle, St. Krückeberg, M. Lindinger, K. Lützenkirchen, L. Schweikhard, H. Weidele, and J. Ziegler, Z. Phys. D **30**, 341 (1994).
[6] G. Dietrich, K. Dasgupta, K. Lützenkirchen, L. Schweikhard, and J. Ziegler, Chem. Phys. Lett. **252**, 141 (1996).
[7] C. Bréchignac, Ph. Cahuzac, J. Leygnier, and J. Weiner, J. Chem. Phys. **90**, 1492 (1989).
[8] C. Bréchignac, Ph. Cahuzac, F. Carlier, M. de Frutos, and J. Leygnier, J. Chem. Phys. **93**, 7449 (1990).
[9] C. Bréchignac, H. Busch, Ph. Cahuzac, and J. Leygnier, J. Chem. Phys. **101**, 6992 (1994).
[10] U. Ray, M. F. Jarrold, J. E. Bower, and J. S. Kraus, J. Chem. Phys. **91**, 2912 (1989).
[11] M. F. Jarrold and K. M. Creegan, Int. J. Mass Spectrom. Ion Processes **102**, 161 (1990).
[12] C. Walther, M. Lindinger, K. Lützenkirchen, L. Schweikhard, and J. Ziegler, Chem. Phys. Lett. **256**, 77 (1996); **262**, 668 (1996).
[13] C. Walther, St. Becker, G. Dietrich, H.–J. Kluge, M. Lindinger, K. Lützenkirchen, L. Schweikhard, and J. Ziegler, Z. Phys. D **38**, 51 (1996).
[14] M. Lindinger, K. Dasgupta, G. Dietrich, S. Krückeberg, S. Kuznetsov, K. Lützenkirchen, L. Schweikhard, C. Walther, and J. Ziegler, Z. Phys. D **40**, 347 (1997).
[15] B. Hammer and J. K. Nørskov, Nature (London) **376**, 238 (1995).
[16] V. Bonačić-Koutecký, L. Češpiva, P. Fantucci, and J. Koutecký, J. Chem. Phys. **98**, 7981 (1993), and references therein.
[17] P. J. Robinson and K. A. Holbrook, *Unimolecular Reactions* (Wiley, London, 1972).
[18] L. S. Kassel, J. Phys. Chem. **32**, 1065 (1928).
[19] P. Fayet, F. Granzer, G. Hegenbart, E. Moisar, B. Pischel, and L. Wöste, Phys. Rev. Lett. **55**, 3002 (1985).
[20] P. Fayet, F. Granzer, G. Hegenbart, E. Moisar, B. Pischel, and L. Wöste, Z. Phys. D **3**, 299 (1986).
[21] T. Leisner, Ch. Rosche, S. Wolf, S. Granzer, and L. Wöste, Surf. Rev. Lett. **3**, 1105 (1996).
[22] I. Katakuse, T. Ichihara, Y. Fujita, T. Matsuo, T. Sakurai, and H. Matsuda, Int. J. Mass Spectrom. Ion Processes **67**, 229 (1985).
[23] I. Katakuse, T. Ichihara, Y. Fujita, T. Matsuo, T. Sakurai, and H. Matsuda, Int. J. Mass Spectrom. Ion Processes **74**, 33 (1986).
[24] A. Selinger, P. Schnabel, W. Wiese, and M. P. Irion, Ber. Bunsenges. Phys. Chem. **94**, 1278 (1990).
[25] C. Jackschath, I. Rabin, and W. Schulze, Z. Phys. D **22**, 517 (1992).
[26] C. Jackschath, I. Rabin, and W. Schulze, Ber. Bunsenges. Phys. Chem. **96**, 1200 (1992).
[27] J. Ho, K. M. Ervin, and W. C. Lineberger, J. Chem. Phys. **93**, 6987 (1990).
[28] G. Ganteför, M. Gausa, K. H. Meiwes-Broer, and H. O. Lutz, J. Chem. Soc., Faraday Trans. **86**, 2483 (1990).
[29] K. J. Taylor, C. L. Pettiette-Hall, O. Chesnovsky, and R. E. Smalley, J. Chem. Phys. **96**, 3319 (1992).
[30] J. Tiggesbäumker, L. Köller, H. O. Lutz, and K. H. Meiwes-Broer, Chem. Phys. Lett. **190**, 42 (1992).
[31] J. Tiggesbäumker, L. Köller, K. H. Meiwes-Broer, and A. Liebsch, Phys. Rev. A **48**, R1749 (1993).
[32] P. Fayet and L. Wöste, Z. Phys. D **3**, 177 (1986).
[33] P. Fayet, W. A. Saunders, and L. Wöste, Hyperfine Interact. **38**, 673 (1987).
[34] S. Wolf, G. Sommerer, S. Rutz, E. Schreiber, T. Leisner, L. Wöste, and R. S. Berry, Phys. Rev. Lett. **74**, 4177 (1995).
[35] S. Krückeberg, G. Dietrich, K. Lützenkirchen, L. Schweikhard, C. Walther, and J. Ziegler, Int. J. Mass Spectrom. Ion Processes **155**, 141 (1996).
[36] S. Krückeberg, G. Dietrich, K. Lützenkirchen, L. Schweikhard, C. Walther, and J. Ziegler, Hyperfine Interact. **108**, 107 (1997).
[37] S. Krückeberg, G. Dietrich, K. Lützenkirchen, L. Schweikhard, C. Walther, and J. Ziegler, Z. Phys. D **40**, 341 (1997).
[38] L. Schweikhard, G. Dietrich, S. Krückeberg, K. Lützenkirchen, C. Walther, and J. Ziegler, Rapid Commun. Mass Spectrom. **11**, 1592 (1997).
[39] V. Bonačić-Koutecký, L. Češpiva, P. Fantucci, J. Pittner, and J. Koutecký, J. Chem. Phys. **100**, 490 (1994).
[40] St. Becker, K. Dasgupta, G. Dietrich, H.-J. Kluge, S. Kuznetsov, M. Lindinger, K. Lützenkirchen, L. Schweikhard, and J. Ziegler, Rev. Sci. Instrum. **66**, 4902 (1995).
[41] G. Savard, St. Becker, G. Bollen, H.-J. Kluge, R. B. Moore, Th. Otto, L. Schweikhard, H. Stolzenberg, and U. Wiess, Phys. Lett. A **158**, 247 (1991).
[42] U. Frenzel, A. Roggenkamp, and D. Kreisle, Chem. Phys. Lett. **240**, 109 (1995).
[43] K. Hansen and E. E. B. Campbell, J. Chem. Phys. **104**, 5012 (1996).
[44] R. A. Marcus, J. Chem. Phys. **20**, 359 (1952).
[45] C. Kittel, *Introduction to Solid State Physics* Wiley, New York, 1976).
[46] S. Krückeberg (unpublished).
[47] *Handbook of Chemistry and Physics*, 71st ed., edited by D. R. Lide (Chemical Rubber Co., Boca Raton, FL, 1990).
[48] M. Manninen, J. Mansikka-aho, H. Nishioka, and Y. Takahashi, Z. Phys. D **31**, 259 (1994).
[49] G. Friedlander, J. W. Kennedy, E. S. Macias, and J. M. Miller, *Nuclear and Radiochemistry* (Wiley, New York, 1981).